One-dimensional physical reference models for the upper mantle and transition zone: Combining seismic and mineral physics constraints

F. Cammarano[1]
Institute of Geophysics, Eidgenössische Technische Hochschule Zürich, Zurich, Switzerland

A. Deuss
Institute of Theoretical Geophysics, Cambridge University, Cambridge, UK

S. Goes and D. Giardini
Institute of Geophysics, Eidgenössische Technische Hochschule Zürich, Zurich, Switzerland

Received 28 June 2004; revised 22 October 2004; accepted 3 November 2004; published 20 January 2005.

[1] One-dimensional seismic reference models are known to be a nonunique solution to global seismic data, hampering an interpretation in terms of physical structure. Here we test the compatibility of the simplest hypothesis of a mantle convecting as a whole, with a constant pyrolitic composition with phase transitions, directly against the kind of seismic data that went into global seismic reference models, focusing on upper mantle structure down to 800 km depth. By randomly varying the elastic and anelastic parameters of the main mantle minerals within their uncertainty bounds, we generate a set of 100,000 adiabatic, pyrolitic models. A small number of these models (<0.1%) give a fit to far-regional *P* and *S* travel times (reprocessed ISC catalog, $\Delta = 18.5°–26°$) and fundamental spheroidal and toroidal modes (reference Earth model Web page, $l > 60$) that is as satisfactory as the fit of preliminary reference Earth model (PREM) or AK135(-F). Although the accepted models have widely different combinations of the mineral parameters, there is a preference for a relatively high olivine shear modulus and its pressure and temperature derivatives, relatively low wadsleyite bulk and shear parameters, and relatively high ringwoodite bulk modulus derivatives. The resulting seismic profiles are very similar and, compared to PREM or AK135, have lower velocities above 400 km, larger jumps near "410," lower transition zone gradients, lower jumps around "660," and stronger gradients directly below. Such physical models that fit seismic data well enough to be useful as a seismic reference model can significantly facilitate physical interpretation of seismic structures.

Citation: Cammarano, F., A. Deuss, S. Goes, and D. Giardini (2005), One-dimensional physical reference models for the upper mantle and transition zone: Combining seismic and mineral physics constraints, *J. Geophys. Res.*, *110*, B01306, doi:10.1029/2004JB003272.

1. Introduction

[2] The knowledge of thermal and compositional structure of the mantle is fundamental for understanding the Earth's internal dynamics. Interpretation of seismological observations in terms of these parameters, based on insights from mineral physics, constitutes the main source of information. With ever improving resolution of three-dimensional seismic models [e.g., *Bijwaard and Spakman*, 2000; *Grand*, 2002; *Masters et al.*, 2000; *Ritsema et al.*, 2004], as well as increasing quality of the mineral physics constraints on elastic [e.g., *Liebermann*, 2000] and anelastic [e.g., *Jackson*, 2000; *Jackson et al.*, 2002] seismic properties at appropriate temperatures, pressures and frequencies, an increasingly comprehensive quantitative physical interpretation is becoming feasible.

[3] Physical interpretation started with the first available spherical seismic models of the Earth. Already *Birch* [1952] and *Bullen* [1975] recognized that the seismic gradients of the upper mantle's transition zone require additional phase and/or chemical transitions. By now, it is well accepted that common mantle minerals do change phase in this depth range and that the dominant mantle mineral, olivine, transforms at the right pressure and temperature conditions to account for the global seismic discontinuities at around 410 and 660 km depth. However, the question whether phase transitions alone are sufficient or whether additional changes in chemistry are required is one that keeps on

[1]Now at Berkeley Seismological Laboratory, University of California, Berkeley, California, USA.

0148-0227/05/2004JB003272$09.00

resurfacing. For example, a recent tomographic study finds indications of global layering of the mantle at 660 km [*Gu et al.*, 2001], which would probably require a change in chemistry at that depth or at least stronger phase transition effects than those given by current mineral physics data. Another recent study proposed that the transition zone is richer in water than the mantle above and below [*Bercovici and Karato*, 2003], a compositional change that should affect seismic velocities. Although, to a first order, the seismic properties of the main discontinuities do correspond to those of the olivine-system phase transitions, it is still debated whether topography, width of the transitions and possibly even depth [*Irifune et al.*, 1998; *Shim et al.*, 2001] agree in detail with these transitions [*Helffrich et al.*, 2003; *Shearer*, 2000; *Xu et al.*, 2003]. Adding to this debate is the fact that it has long been recognized that the jump around 410 km in the most common seismic 1-D models is less than that predicted for a pyrolitic mantle [*Katsura et al.*, 2004; *Stixrude*, 1997]. Some authors [e.g., *Duffy and Anderson*, 1989] have interpreted this as an indication of a different (less olivine-rich) mantle composition. Others [*Ita and Stixrude*, 1992; *Jackson and Ridgen*, 1998; *Weidner*, 1985] found the uncertainties in seismic models and/or mineral physics data large enough to accommodate the difference. Also the seismic jumps around 660 km depth are somewhat different from those given by a pyrolitic model. The difference is less than at 410 and is generally attributed to a significant gradient below the ringwoodite to perovskite + magnesiowüstite transition due to the transformation of garnet, which may be partially mapped into the jump in the seismic models due to a lack of depth resolution.

[4] Often forgotten in these discussions is that transition zone structure is actually not well resolved by the data that went into the most commonly used global reference models, AK135 [*Engdahl et al.*, 1998; *Kennett et al.*, 1995] and PREM [*Dziewonski and Anderson*, 1981]. Furthermore, the structure of these seismic models is influenced by the chosen parameterization. The model AK135 was constructed as a reference model for travel time data to be used for, for example, earthquake relocation problems and seismic phase identification. AK135 was derived from fitting ISC travel time data for *P* and *S* waves at distances beyond those where the transition zone triplications affect the picks. It comprises isotropic *P* and *S* velocity profiles. A modification, AK135-F [*Montagner and Kennett*, 1996], also includes a density and anelasticity structure, derived by adding constraints from normal mode data. The Preliminary Earth Reference Model (PREM) is dominated by the constraints from free oscillation frequencies and surface wave dispersion curves, but also included a set of *P* wave and *S* wave travel times. In addition, the model was constrained to fit the Earth's mass and moment of inertia. PREM gives V_P, V_S, density, and anelasticity and radial anisotropic structure for both *P* and *S* velocities. Both AK135 and PREM are widely used and give very good first-order fits to travel times and mode data, respectively. Seismically, there has been little reason to update them, apart from possibly eliminating the 220 km discontinuity in PREM, which many people now think is not a global isotropic feature [*Deuss and Woodhouse*, 2002; *Gung et al.*, 2003; *Leven et al.*, 1981].

[5] However, for the physical interpretation of seismic structure there is reason to reevaluate these models. Under upper mantle conditions, seismic velocities depend nonlinearly on temperature due to the influence of anelasticity [*Cammarano et al.*, 2003; *Karato*, 1993; *Sobolev et al.*, 1997], which means that one needs absolute velocities for a thermal interpretation. Not all seismic inversions are sensitive to the one-dimensional background structure. For example, regional teleseismic travel time models mainly resolve anomalies relative to the (unknown) one-dimensional average structure below the stations. Furthermore, most seismic inversions are damped toward a starting model that very often is one of the global reference models. Thus a good understanding of one-dimensional seismic structure is crucial for physical interpretation. Temperature has a dominant influence on upper mantle seismic structure, but other parameters (chemistry, fluids, and melt) may contribute as well. To separate these effects, one often compares relative anomalies in *P*, *S* velocity and density [e.g., *Cammarano et al.*, 2003; *Karato and Karki*, 2001; *Masters et al.*, 2000; *Saltzer et al.*, 2001], as the different seismic parameters have different sensitivities to the various physical parameters. For this too, it is crucial that one understands what the reference structure means, and whether reference V_P, V_S and density actually correspond to the same physical conditions.

[6] Our aim in this paper is to define a physical one-dimensional model for the upper mantle that can be used for seismic inversions and aid their interpretation. Our analysis is an illustration of how this problem can be approached and gives a first set of physical reference models. These models can certainly be improved with better mineral physics constraints, different seismic data sets (that provide better transition zone constraints), and possibly with a more comprehensive search of the model space. However, even the current setup already provides insight into the constraints on average upper mantle structure.

[7] The simplest hypothesis for a reference physical structure is that of a mantle with constant composition, pyrolite with phase transitions, and convecting as a whole, i.e., with a thermal boundary layer at the mantle's top (and base), and adiabatic in between. We test whether such a structure is, within the uncertainties of mineral physics data, consistent with data similar to those used in the common 1-D reference models, i.e., seismic travel times (direct *P* and *S*) and fundamental mode frequencies (both spheroidal and toroidal). We find a set of models that satisfy mineral physics constraints on elastic and anelastic parameters of mantle minerals as well as seismic data. In this paper, we treat the upper mantle and transition zone, extending our models to 800 km depth to encompass all phase transitions of major upper mantle minerals (for simplicity, we will refer to this as the upper mantle in the rest of the paper). The lower mantle is investigated separately (Cammarano et al., manuscript submitted to EPSL).

2. Method

[8] To help describe the method used in this paper, we may think of our problem as a typical inverse problem $\mathbf{A} \cdot \mathbf{x} = \mathbf{b}$ that treats the seismic data as the data vector $\mathbf{b}$, and the mineral physics parameters as the solution vector $\mathbf{x}$. Model description $\mathbf{A}$ relates the mineral physics parameters for a pyrolitic, adiabatic mantle to seismic structure. Uncertainty ranges in the experimental and theoretical elastic and

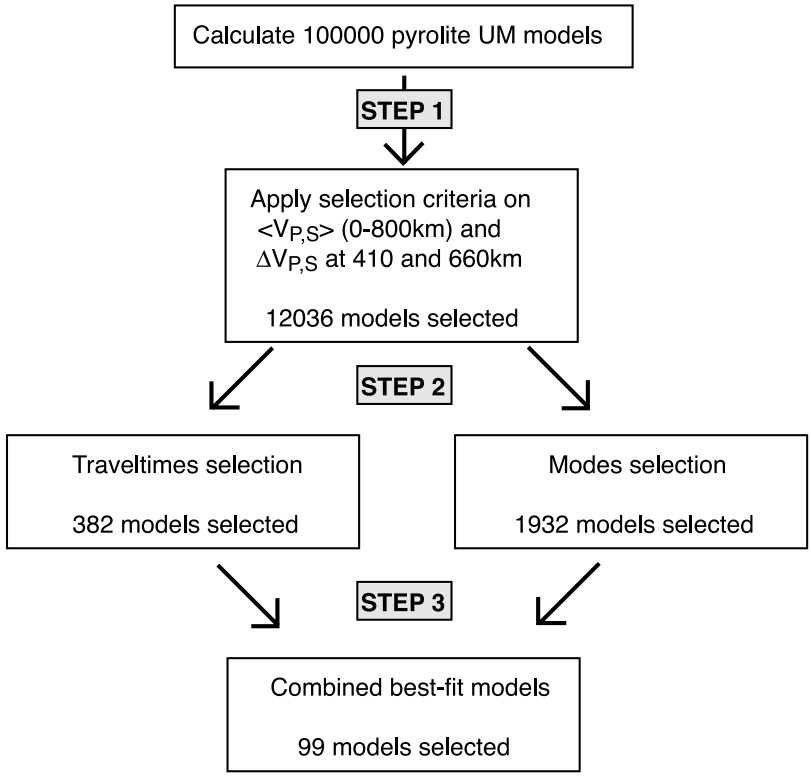

Figure 1. Flowchart illustrating the steps in our inversion procedure.

anelastic mineral parameters as determined by *Cammarano et al.* [2003] bound the considered solution space. Our problem is very nonlinear, and we cannot set up an actual matrix of partial derivatives **A**. Instead, we forward calculate synthetic seismic profiles from sets of mineral physics parameters chosen in a Monte Carlo search of the solution space. The resulting profiles are evaluated for their compatibility with the seismic data. This ''inversion'' is done in three steps (see the flowchart in Figure 1). In the first step, selection criteria based on independent seismic constraints on average upper mantle velocities and discontinuity jumps narrow the search space significantly without calculating full fits to the seismic data. In the second step, we test the fit of this narrowed down pyrolite model set to the travel times and normal mode frequencies, independently. In the third step, models that provide a satisfactory fit to both types of seismic data are selected and the solutions are analyzed.

2.1. Physical Model

[9] As a physical model, we chose a pyrolitic mantle with the thermal structure of a 60 m.y. old oceanic lithosphere and an adiabat with a potential temperature of 1300°C below. Pyrolite is the most widely accepted (although not the only) model of mantle composition, and generally compatible with a large range of petrologic, geochemical and seismic observations [*Ringwood*, 1975]. The pyrolite composition at surface conditions used, is: 61.7% Olivine, 15.3% Garnet, 13.3% CPX, 5.2% OPX, 4.5% jadeite [*Irifune and Ringwood*, 1987]. Slightly different versions of pyrolite will not modify our results as seismic velocities have only limited sensitivity to composition at upper mantle depths [*Cammarano et al.*, 2003], especially to variations as small as the differences between pyrolitic models. The changes in mineralogy with depth are computed according to the experimental phase diagrams compiled by *Ita and Stixrude* [1992]. Uncertainties in these phase diagrams are not taken into account in our current analysis, although they may be significant (for instance, errors of around 0.5 GPa, circa 15 km, in transition pressure are not unusual (D. Frost, personal communication, 2002)). Phase diagrams determined in thermodynamic equilibrium calculations [e.g., *Bina and Helffrich*, 1992; *Connolly and Petrini*, 2002; *Mattern et al.*, 2003] would allow for a better propagation of errors, but still have large uncertainties due to the limited availability of the necessary experimental parameters and the uncertain influence of secondary components.

[10] For the thermal structure we decided to use the simpler oceanic situation (without radiogenic heat production) as a reference structure, and chose an oceanic lithosphere of medium age. This thermal structure intersects that of the mantle adiabat at circa 110 km depth. The potential temperature of the convecting mantle is relatively tightly constrained around 1300°C (within ±50°C) from the petrogenesis of mid-ocean ridge basalts [e.g., *Green et al.*, 1999]. Variations in adiabatic temperatures due to different choices of the mineral parameters are generally small, on the order of 10°.

[11] The model does not include a physical reference for the crust. The large lateral variations in crustal structure hamper defining a useful physical reference structure. Instead we use PREM's global average structure (for the travel time calculations without water layer) with a crustal thickness of 24 km and average V_P and V_S (below the water layer) of 6.175 and 3.462 km/s, respectively. For fitting the

ISC travel times we find that we need to modify the crustal structure to a more continental one, as discussed below. Although not as variable in composition as the crust, the lithosphere also exhibits significant lateral variability down to about 350 km depth [*Röhm et al.*, 2000; *Ritsema et al.*, 2004], including possibly systematic variations in chemistry between oceanic and (old) continental lithosphere. However, the seismic data we use are mainly sensitive to average crust plus lithosphere structure. Therefore we decided to keep one physical reference structure for the lithosphere and modify only the crust for continent-ocean differences if necessary.

[12] Finally, we test an isotropic physical reference model. Seismic anisotropy may be considerable, especially at shallow mantle depths. However, there is no obvious physical one-dimensional reference model for the amount and orientation of anisotropy. Although the intrinsic anisotropy of the main mantle minerals is known, the resulting large-scale anisotropy depends on stress, strain, temperature, deformation mechanism and water content [*Karato*, 1998]. The choice of an isotropic model will somewhat hamper the simultaneous fit of spheroidal and toroidal modes.

2.2. Seismic Data

[13] The travel times used are direct *P* and *S* phase travel times from the reprocessed catalog [*Engdahl et al.*, 1998; E. R. Engdahl, personal communication, 2001] which is based on ISC data until 2000 (for simplicity, we will refer to this data set as ISC data). Only the highest quality data in the catalog have been included in our analysis (those marked as having a precision of 1/10 of a second). The catalog contains ten times more *P* (1,021,214) than *S* (110,225) arrivals and the quality of the *P* data is better. *S* residuals may contain biases because they may be affected by phase misidentifications and were not used in the reprocessing. We minimize the misfit of data at far-regional epicentral distances, between 18.5° and 26° for *P*, and 19.5° and 26° for *S*, thus excluding the arrivals of *Pn* and *Sn* at shorter epicentral distances. These phases directly sample the transition zone with rays turning below 300 and above 800 km depth. Above 300 km only the average structure contributes to the data fit, i.e., we cannot differentiate between crustal and lithospheric structure. Identifying arrivals at far-regional distances is complicated by triplications. For this reason, AK135 minimized only the misfit of data at epicentral distances larger than 25°. However, the scatter of the reprocessed travel times before 26° is only slightly higher than that of arrivals at larger distances and the distribution in each distance interval is close to Gaussian, showing no obvious skew because of picks of a later triplication branch. We use the standard deviation of the scatter as an estimate of travel time uncertainty. Despite the large number of data, spatial coverage at these epicentral distances is sparse and strongly biased toward continents and subduction zones.

[14] Normal mode mean frequency data have been selected from the REM (reference Earth model) Web page (http://mahi.ucsd.edu/Gabi/rem.html). Our physical reference models only have structure up to 800 km depth, so we selected normal modes with sensitivity above 800 km. This corresponds to fundamental branch modes with angular order larger than 60; we did not include overtones which have deeper sensitivity. Both spheroidal (i.e., corresponding to Rayleigh waves at periods 50–153 s) and toroidal (corresponding to Love waves at periods 58–139 s) modes have been used. Note that these data are especially sensitive to structure in the shallow mantle above 400–500 km depth and have only a limited sensitivity to the deepest transition zone. We compute the normal mode frequencies and compare with the observations. This is equivalent to comparing phase velocities and dispersion curves. The data set is similar as was used for the PREM model, but PREM only included spheroidal modes/Rayleigh waves up to 61 s and toroidal modes/Love waves up to 125 s. It also constitutes an update compared to the frequency values used in AK135-F.

2.3. Mineral Physics Data

[15] Seismic velocities depend on the elastic shear and bulk modulus, density and anelasticity (intrinsic seismic attenuation, due to nonelastic energy loss). For the Monte Carlo search we allow the elastic bulk and shear modulus, their pressure and temperature derivatives and thermal expansion to vary within the uncertainties bounds defined by *Cammarano et al.* [2003]. We do this for the magnesium end-members of six upper mantle minerals: olivine, wadsleyite, ringwoodite, clinopyroxene, orthopyroxene and garnet, and three lower mantle minerals: perovskite, magnesiowüstite and calcium-perovskite. Some parameters that have only a minor influence on seismic velocities are kept fixed to the average values of *Cammarano et al.* [2003]. These are density at zero pressure and temperature (which has very small uncertainty bounds), the properties of the iron end-members and other minor constituents: jadeite, grossular garnet and Na-majorite. These choices were made after testing the sensitivity of seismic velocities to the various elastic mineral parameters. We find that velocities are significantly sensitive to all parameters we changed. Although seismic velocities will change most when zero-pressure bulk and shear moduli are changed (e.g., for olivine, a 0.2 to 0.5% velocity change for a 1% change in modulus), the uncertainties in the pressure and temperature derivatives are an order of magnitude larger (around 10%) giving them a similar total effect on velocity (0.3–1.2% for olivine). The sensitivity to an individual parameter is complex, as it changes as a function of pressure and temperature as well as in conjunction with the values of other parameters. These tests also emphasize the very nonunique relation between seismic velocities and mineral parameters, allowing the same variations in seismic velocity to be achieved by many possible combined variations in mineral parameters.

[16] In addition, we randomly choose shear anelasticity models from a set of eight models defined by *Cammarano et al.* [2003]. The anelasticity models differ in their depth and temperature dependence, based on the limited set of experimental constraints. For an adiabat with a 1300°C potential temperature, they all give attenuation curves that are within the range of 1-D seismic attenuation models. Bulk attenuation is kept fixed as in *Cammarano et al.* [2003]. We do not include any frequency dependence of Q (although this is in the original models defined by *Cammarano et al.* [2003]) and use the 1 Hz values.

Frequency dependence of Q has been thought to be weak and is commonly neglected (as in PREM and AK135) [e.g., *Aki and Richards*, 2002]. Recent seismological work [e.g., *Cheng and Kennett*, 2002; *Shito et al.*, 2004] and laboratory studies [*Jackson*, 2000] have found that frequency-dependent effects may be more significant. However, because of the large uncertainties in the anelasticity parameters, and trade-offs between frequency and depth dependence at a given reference frequency [*Oki et al.*, 2004], we decided to use a simplified Q parameterization, without frequency dependence, and include uncertainties through the use of a set of seismically reasonable Q profiles. Frequency-dependent anelasticity affects a combined body wave and normal mode fit. However, because our body wave and normal mode data sets have their main sensitivity in complementary parts of the upper mantle, we do not think this choice will have a significant effect on our final conclusions. For more detail on the constraints for the mineral parameters and a full list of references, we refer to *Cammarano et al.* [2003]. Altogether, a total of 70 parameters are varied.

2.4. Forward Calculation of Seismic Velocities

[17] Using the mineral physics parameters, velocities were calculated at appropriate pressure and temperature conditions in four steps [*Cammarano et al.*, 2003]: (1) elastic mineral parameters are extrapolated in temperature for zero pressure, (2) high-temperature elastic parameters are extrapolated in pressure along an adiabat using a Birch-Murnagham equation of state (EOS), (3) A Hashin-Strikman averaging of the high pressure and temperature parameters gives elastic velocities and density for the mineralogy according to the phase diagram, (4) the temperature and pressure-dependent effect of anelasticity is added. Above 660 km depth, we use a linear temperature correction and a third-order EOS like *Cammarano et al.* [2003]. Below 660 km depth, a nonlinear temperature extrapolation using the Anderson-Grüneisen parameter and a fourth-order EOS are applied. Although the higher order extrapolation is not critical down to 800 km depth, it is more appropriate for the lower mantle (F. Cammarano et al., manuscript in preparation, 2004). As the second-order pressure derivatives for bulk and shear modulus are also needed when a fourth-order EOS is used, there are nine elastic parameters to be varied for each lower mantle mineral, while there are only seven per upper mantle mineral.

2.5. Inversion Procedure

[18] By randomly varying the mineral physics parameters within their uncertainty bounds, we define a set of 100,000 upper mantle models. This number of models does not constitute an exhaustive exploration of the parameter space, which at the moment is computationally unfeasible. For example, in our case, 70 parameters are varied: if one allows each one to assume one of ten fixed values, the number of combinations will be 10^{70}, the so-called "curse of dimensionality". However, the solutions found for different subsets of the explored model space are very similar and therefore our conclusions in locating the key mineral physics parameters are robust. More caution is to be used in analyzing the correlation between the parameters involved, but some general inferences can be made as well.

[19] Other global search procedures, such as genetic algorithms, simulated annealing or the neighborhood algorithm [*Sambridge*, 1999, and references therein], could do a similar job as our Monte Carlo type inversion. Our search is optimized by the use of a priori seismic information, which on the one hand saves a lot of computing time, and on the other allows a selection of the best individuals in the population. Other methods would require tuning to deal with the complicated fitness landscape in our problem, where the relation between mineral physics parameters and seismic data is extremely nonlinear, and parameter trade-offs lead to a set of quite different minima spread widely across the solution space. For a complete review of the pros and cons of different inversion strategies, see *Sambridge and Mosegaard* [2002].

3. Results

[20] We discuss the results of our inversion and show what the selectivity is of each of the steps (Figure 1) of the procedure.

3.1. First Selection

[21] In a first step, we discard all models that do not satisfy a set of basic seismic selection criteria (Table 1). We found that these characteristics of the models are important for a reasonable seismic fit. Although the ISC travel time data and the fundamental mode data set do not strongly constrain the detailed velocity gradients and jumps in the upper mantle, they do put significant constraints on the average velocities for the whole depth interval 0–800 km. Average V_P and V_S, $\langle V_P \rangle$ and $\langle V_S \rangle$, of AK135, AK135-F and PREM are all very close (Figure 2a). Only pyrolite models with a $\langle V_P \rangle$ of 9.195 ± 0.5% km/s and $\langle V_S \rangle$ of 5.055 ± 0.9% km/s are kept (Table 1). These bounds include a reasonable range of average velocities when one looks at the range of the seismic reference models. However, the ISC travel times and normal mode frequency data may be sampling a different average crustal structure due to the continental distribution bias of the travel time data. The large bounds allow for significant uncertainty in crust+lithosphere structure.

[22] Regional seismic studies of the amplitude jumps at around 410 and 660 km depth give a large range of values. *Shearer* [2000] compiled data from various upper mantle velocity models in different (mostly continental) regions. This compilation gives generally larger V_P and V_S jumps at 410 km than those in the PREM and AK135 models. The global seismic data we use are not sensitive to details of the velocity distribution around the mantle discontinuities. Pyrolite models with a very large jump at the olivine-wadsleyite transition, however, do give a poor fit to the seismic data, as a large jump implies very high transition zone velocities that need to be compensated by slow velocities above 400 km to preserve average velocities. Furthermore, a large jump introduces considerable structure in the travel time residuals (see below). Therefore we rejected models with jumps much larger than the range found by *Shearer* [2000] and discard those that have a larger ΔV_P or ΔV_S than 8.5% (compare with PREM 2.54% for ΔV_P and 3.35% for ΔV_S, and AK135 and AK135-F 3.59% for ΔV_P and 4.22% for ΔV_S) (Figure 2b and Table 1). There

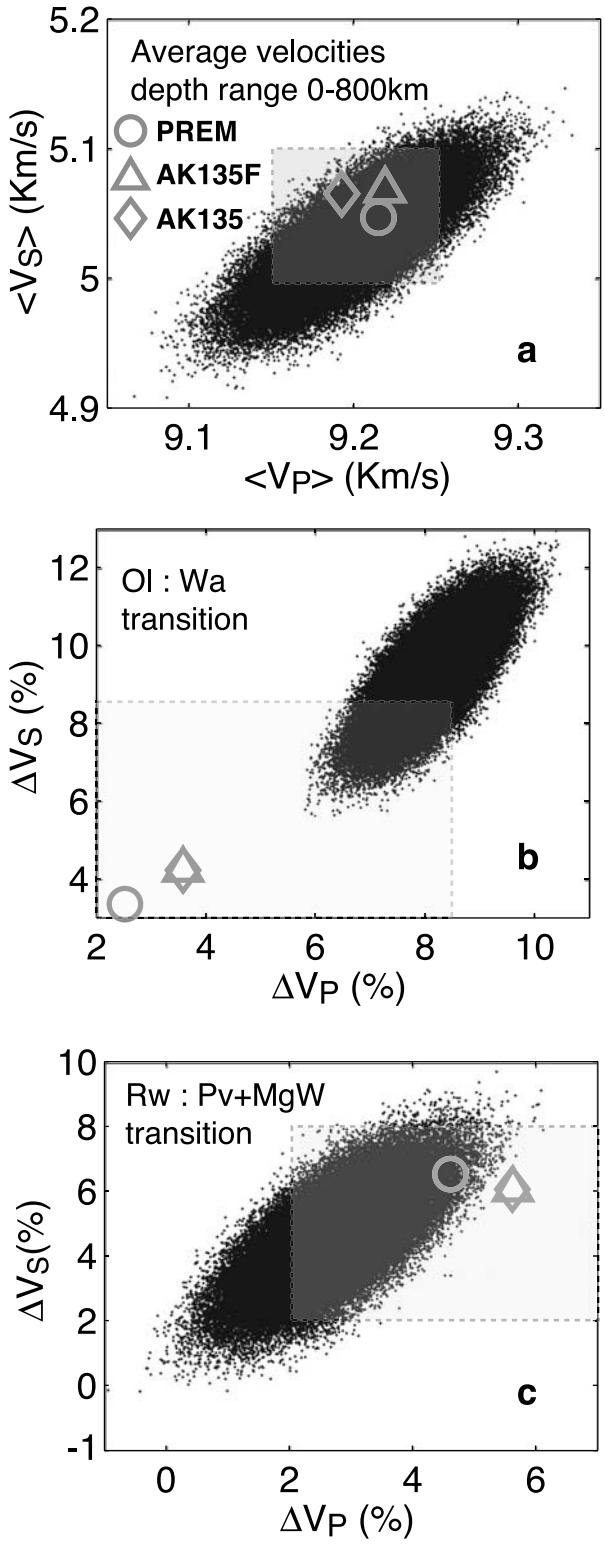

Figure 2. (a) Average velocities and (b) amplitude jumps for the olivine to wadsleyite transition (~410 km depth) and (c) the ringwoodite to perovskite+magnesiowüstite (~660 km depth) for the initial 100,000 pyrolitic models compared with values from PREM (circles), AK135 (diamonds), and AK135-F (triangles). The selection bounds applied in the first step are marked by the dashed rectangles.

is a better agreement between the seismic and pyrolite velocity jumps at 660 km, especially for ΔV_S (Figure 2c). On the basis of Shearer's compilation we again reject pyrolite models with jumps that are too extreme (Table 1), in this case mainly those that have too small a ΔV_P (<2%), a small portion of the models.

[23] We also applied some constraints on the density average and jumps, but these do not reject any of the models (Table 1). Most selective are the constraints on the jump in ΔV_S at 410 km depth. Only about 12% (12,036) of the initial 100,000 models pass these first selection criteria. The degree of selectivity and the remaining set of models is very similar for a subset of only 10,000 models, giving us confidence in the stability of these results. Subsequently, we calculate the fit of all models that pass this first step to travel times and normal mode frequencies (Figure 1).

3.2. Step 2: Travel Time Data Fit

[24] Figure 3 shows the mean and standard deviation of the ISC travel time data relative to AK135. Also shown are the same data relative to AK135 after applying ellipticity and station (path averaging) corrections [*Engdahl et al.*, 1998]. These corrections give only a minor reduction of the scatter. Note that in the distance range where the AK135 misfit was minimized, the residual curve is almost flat, and *P* residuals are close to 0s, but AK135 is almost 1s fast compared to the average of the more poorly constrained *S* travel times. In the far-regional distance range, where data sample only the upper mantle, there is structure to the mean residuals. Mean *P* residuals to PREM show a similar trend with structure in the distance range <25°, and a flat residual beyond. In addition, there is a systematic offset of about +1s. *Antolik et al.* [2001] find that a correction for three-dimensional crustal *P* velocity structure using CRUST 5.1 [*Mooney et al.*, 1998] largely removes this shift (slightly overcompensating it), without influencing the residuals' structure significantly. A similar shift can also be achieved by lowering average crustal V_P by a uniform 12% relative to PREM's global average, without changing crustal thickness, a velocity difference similar to the difference between an average continental crustal velocity and PREM. This emphasizes the continental bias of the travel time data at far-regional distances, and shows the considerable effect that crustal (+lithospheric) structure can have on the average

Table 1. First Selection[a]

	Constraints		Selectivity, Percent of Models Selected	
	Min	Max	10^4 Models	10^5 Models
$\Delta V_P 410$	2	8.5	73.19	72.3
$\Delta V_S 410$	2.5	8.5	22.95	23.4
$\Delta\rho 410$	2	12	100	100
$\Delta V_P 660$	2	8	81.34	81.02
$\Delta V_S 660$	2	8	89.69	89.46
$\Delta\rho 660$	2	14	100	100
$\langle V_P \rangle$ (0–800 km)	9.15	9.24	82.83	82.86
$\langle V_S \rangle$ (0–800 km)	5.01	5.10	75.50	75.43
$\langle \rho \rangle$ (0–800 km)	3.71	3.75	99.97	99.98
Total			11.87	12.04

[a]Constraints are used for amplitude jumps at mantle discontinuities and average velocity (depth range 0–800 km). Note the similarity between the subset of 10^4 models and the total 10^5 models computed. Note 12,036 models out of 100,000 pass the first selection.

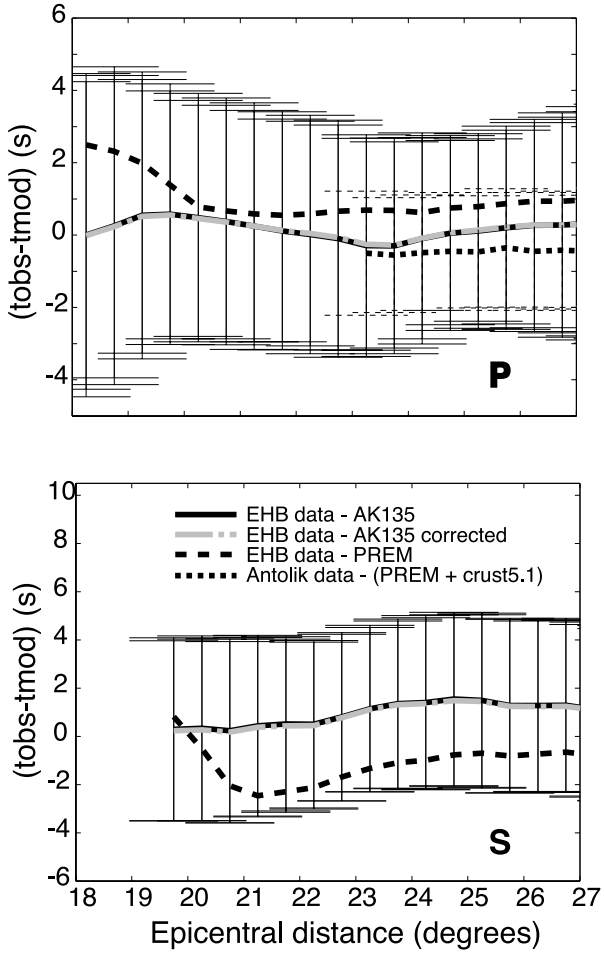

Figure 3. Travel time summary data from the reprocessed ISC catalog for 1964 through 2000 [*Engdahl et al.*, 1998]. Travel times relative to AK135 for events between 5 and 15 km depth are averaged over 0.5° intervals to obtain the shown mean and standard deviations. For comparison, *P* wave travel times corrected by *Antolik et al.* [2001] for crustal structure and travel times relative to PREM are also shown.

residual of the travel time data. PREM far-regional *S* residuals are overall low and show more structure which persists to distances as large as 40°. Note that all residuals were determined relative to isotropic PREM. Including PREM's radial anisotropy may give somewhat different residuals, because of predominantly steep incidence angles in the distance range we investigate.

[25] The residuals for the pyrolitic velocity models are illustrated for 1000 of the 12,036 models in Figure 4. The models not shown have similar residuals. Travel times for the models have been calculated by full ray tracing using the times code (from IASPEI web page). For comparison, the residuals to AK135 and PREM are shown again and the residual to AK135-F is added. The average offsets of the residual curves span a large range, reflecting the relatively broad bounds on average seismic velocity used in the first step. The *P* models have a systematic positive offset, whereas *S* average residuals also attain values less than 0. As the seismic models, the synthetic model residuals also have a pattern in the far-regional distance range, but it differs from the seismic model patterns. The shape of this pattern is related to structure between 300 and 800 km, while the offsets are mainly the effect of shallower structure. The relatively well-constrained bulk modulus properties of mantle minerals, result in a similar trend for all *P* models, reflecting that the pyrolite models generally have lower velocities than the seismic models above 410 and higher velocities below. The residual patterns of the *S* models are more variable and show a less strong structure. Note that the models rejected in the first step because of their too large jump at 410 would give residuals with an even stronger structure.

[26] We separate the measure of misfit in two parts, a mean offset characterizing the misfit of PREM crust plus mantle structure above 300 km, and a standard deviation relative to this mean that characterizes the misfit due to structure between 300–800 km depth. As the pyrolite models do not include a physical reference structure for

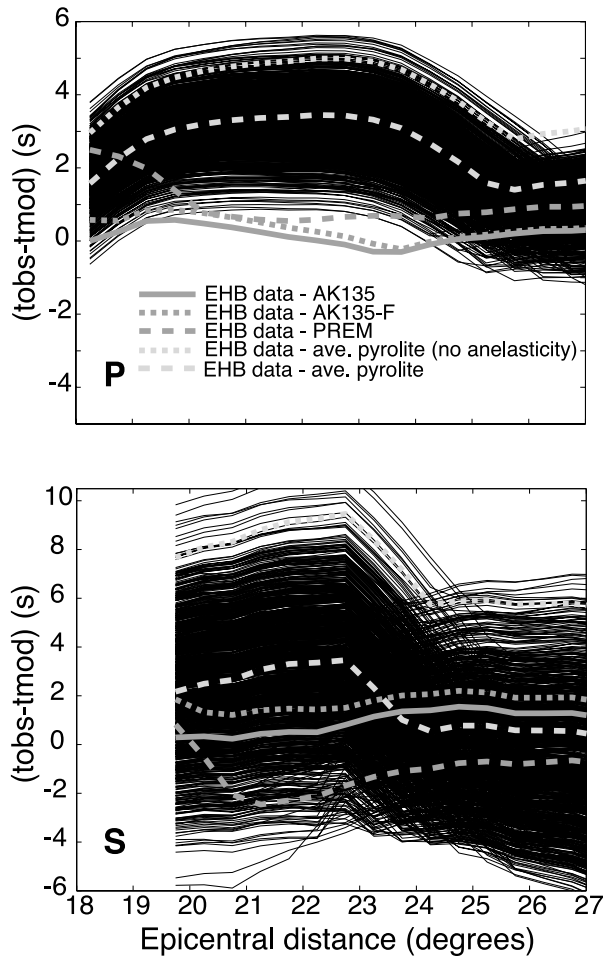

Figure 4. P and *S* travel time residuals relative to AK135 of 1000 pyrolite models, representative of the fit of the full 100,000 set, compared with the mean data residuals relative to AK135 (solid gray line), PREM (long-dashed line), and AK135-F (short-dashed line). Light gray lines are mineralogical models with average properties with (long-dashed) and without (short-dashed) anelasticity (anelasticity model Q5).

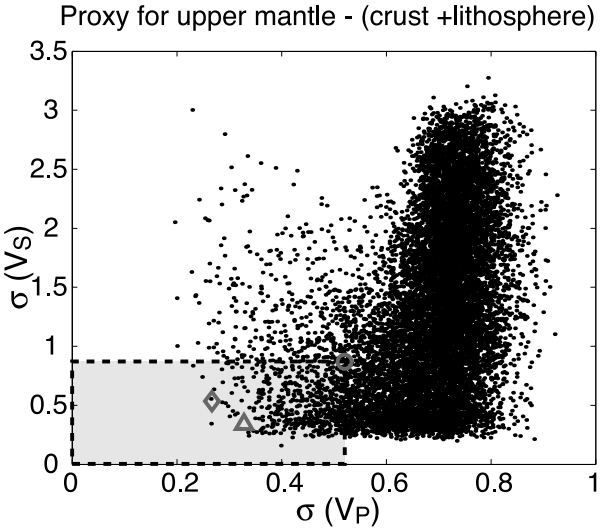

Figure 5. Standard deviation of *P* and *S* residuals of all pyrolite models relative to their mean, compared with structure of PREM (circle), AK135 (diamond), and AK135-F (triangle) residuals. Here σP and σS are a proxy for the fit to upper mantle structure between 300 and 800 km depth, i.e., without crust and lithosphere. The gray box marks the limits used for selecting acceptable models.

the crust, and it is already clear that PREM's global crust is too fast for travel times, we are mainly concerned with choosing models with low standard deviation of the residual structure. We reject all models that have a standard deviation that is larger than that of PREM (Figure 5 and Table 2). This leaves only 0.4% of the original 100,000 models.

[27] Accepting these low residual standard deviation models implies that we think we can find an acceptable alternative for the shallow structure that will shift the residuals to be around 0s. To check this, we invert for the necessary correction to average crustal velocity, keeping the crustal thickness fixed to the value of 24 km. This allows us to use a physical 1-D structure for the lithosphere and maps any necessary shift due to a bias of the data distribution to the continents into average crustal velocities, $\langle V_{P,S}\rangle_c$. We compare the obtained crustal velocity values with those from the crustal model CRUST2.0 [*Bassin et al.*, 2000], converted to average values for a 24 km thick crust (Figures 6a and 6b). The bimodal distribution of CRUST2.0 average velocities is due to the contribution of continents (lower velocities) and oceans. We expect the crustal velocities necessary for shifting the residuals to lie on the continental side, and will reject models that require an excessive shift (Table 2). Note the travel time calculations used PREM crust without the water layer.

[28] Indeed, the inverted values of $\langle V_S\rangle_c$ (Figure 6d) overlap with the continental peak of CRUST2.0. The shift of $\langle V_P\rangle_c$ (Figure 6c) toward relatively low crustal averages is due to the chosen 24 km thickness, which is small for continental crust. As a result, the depths between 24 and 30 or 40 km contain very high lithospheric velocities (due to the cool geotherm at these shallow depths). The low crustal velocities compensate for this. Note also that PREM *S* residuals do not require the strong crustal correction that the *P* data indicate (Figure 4). The less extreme shift required for $\langle V_S\rangle_c$ could be affected by systematic biases in the *S* travel times due to sparser distribution, picking or reprocessing. Furthermore, crustal *S* velocities in CRUST2.0 are less well constrained than V_P and often inferred from a scaling relation between V_P and V_S. Only the models that require the most extreme crustal corrections (Figure 6 and Table 2) are rejected, leaving 382 selected models, i.e., slightly less than 0.4% of the original model space. This crustal inversion aims at determining the reliability of the upper mantle models and not at providing an alternative reference crustal structure. Although not optimal, this procedure is acceptable for the travel time data that sense only average velocity and not detailed structure above 300 km. The crustal corrections show that the required shallow mantle average velocity can be reconciled with continental structure. For the normal mode frequencies that do have sensitivity to the shallower structure, an oceanic base model is a reasonable choice. Ultimately, a global reference model may need to at least include a continent-ocean dichotomy [*Dziewonski et al.*, 1975]. Such a physical model would probably reject even more parameter combinations.

[29] For the models shifted according to $\langle V_{P,S}\rangle_c$, we calculate a far-regional misfit between data and model using the same criterion as was used for AK135 [*Engdahl et al.*, 1998; *Kennett et al.*, 1995]:

$$\psi_{P,S} = \frac{1}{N_{P,S}} \sqrt{\left[\sum_{j=1}^{N_{P,S}} \left(\frac{t_j^{obs} - t_j^{mod}}{\sigma_j}\right)^2\right]}, \qquad (1)$$

where $N_{P,S}$ is the total number of measurements, t_j^{obs} is the travel time observed, t_j^{mod} is the computed travel time for each model, and σ_j is the standard deviation of the data spread (see Figure 3). Figure 7 shows the misfit for all models from step 1 and those rejected based on shape misfit and crustal correction. The misfit of the selected models is very acceptable when compared with seismic models. Note that this misfit is not used for rejecting models.

3.3. Step 2: Normal Mode Frequency Fit

[30] Independently, we analyzed the models that passed step 1 for their fit to the fundamental mode frequencies. The normal mode central frequencies are calculated by solving the differential equations governing free oscillations and using numerical integration [*Woodhouse*, 1988]. The mean frequency measurements correspond to the

Table 2. Second Selection, Travel Time Based[a]

	Constraints	Selectivity, Percent of Models Selected
σ(*P*) (18.5°–27°)	<0.5206	7.70
σ(*S*) (19.5°–27°)	<0.8681	31.48
$\langle V_P\rangle$ (0–24 km)	>4.0, <6.0	90.31
$\langle V_S\rangle$ (0–24 km)	>2.4, <3.7	80.20
Total		3.174

[a]Here σ(*P*, *S*) are the standard deviation from each model's mean, related to TZ structure. $\langle V_{P,S}\rangle$ are the inverted values for the 24 km thick layer on top of our models that give the optimum fit to data. The percentages refers to the 12,036 models; 382 models out of 12,036 are selected.

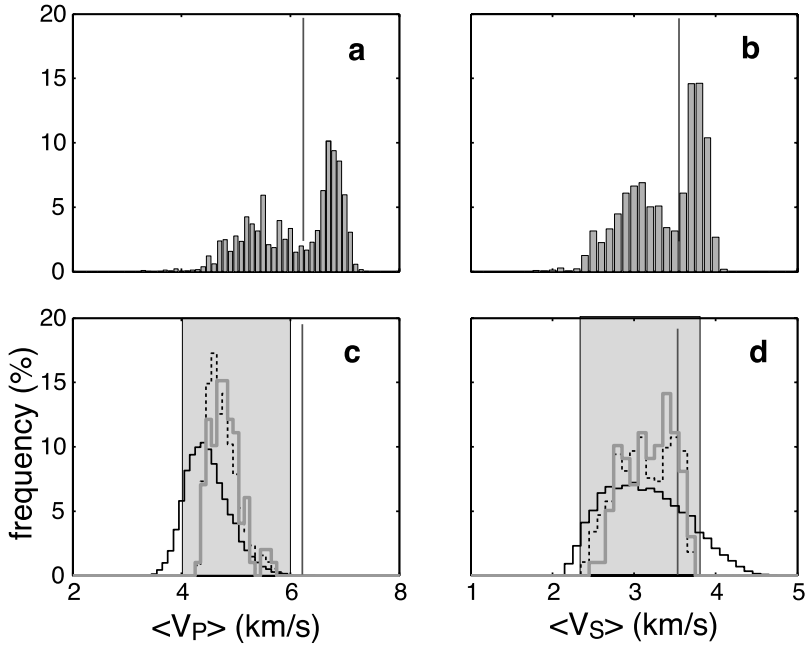

Figure 6. Average crustal velocity for the CRUST2.0 model [*Bassin et al.*, 2000] converted to a constant crustal thickness of 24 km for (a) V_P and (b) V_S. (c and d) Average crustal velocity necessary to optimize the travel time fit of the 12,036 models that pass the first selection (solid line), the 382 models with the best travel time fit σ(P) and σS (dashed line), and the 99 best fit models after the full inversion (gray line). Only the average crustal velocities were varied, while crustal thickness was fixed to 24 km and lithospheric structure follows that of a 60 m.y. old oceanic lithosphere. Vertical gray lines indicate starting values (PREM crustal structure). The gray box shows the limits of accepted crustal corrections.

degree-zero part of phase velocity maps, and are only sensitive to spherically averaged Earth structure. The aspherical structure (degree larger than zero) in the phase velocity maps is sensitive to crustal and upper mantle structure. By only using the mean frequencies, we average the influence of lateral velocity variations in the crust and continental versus oceanic differences (which are dominated by degree 2 structure). So for the normal mode data we do not have the same complications with crustal structure as for the travel time data.

[31] We aim to find models with a misfit to the normal mode frequencies as acceptable as the misfit for the PREM model. The misfit function is similar to the one used for the travel time misfit. Anisotropy is needed to reconcile Love and Rayleigh wave data [*Dziewonski and Anderson*, 1981]. Consequently, transverse (vertically symmetric) isotropy was introduced in PREM above 220 km depth to improve the total data fit to short period spheroidal and toroidal mode data. We compared the misfit for anisotropic PREM with its Voigt average isotropic equivalent to investigate the influence of anisotropy. Figure 8 shows the misfit between the REM best estimate mean frequencies and the anisotropic and isotropic versions of the PREM model. The anisotropic-PREM fit for the spheroidal modes is slightly worse than that of isotropic PREM, while anisotropy results in significant improvement of the toroidal mode misfit. We also show the misfit for the (isotropic) AK135-F model, which was obtained from AK-135 by adding normal mode frequencies to the inversion [*Montagner and Kennett*, 1996]. We

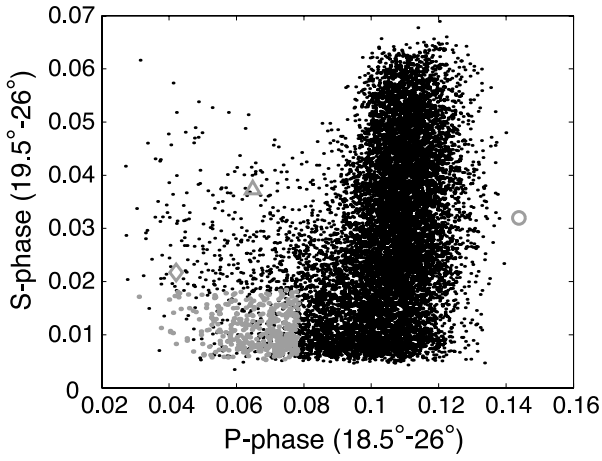

Figure 7. Upper mantle misfit criterion similar to that used in determining AK135 [*Kennett et al.*, 1995] for *P* and *S* phases of the 12,036 models that pass the first selection (in solid dots) and 382 best fit (σP and σS) travel time models (in gray dots). The inverted 1-D crustal velocities for each model are used. This misfit is sensitive to upper mantle structure from the surface to 800 km, including crust and lithosphere. It is not used for model selection. Misfits of the seismic models are shown for comparison: PREM, circle; AK135, diamond; AK135-F, triangle.

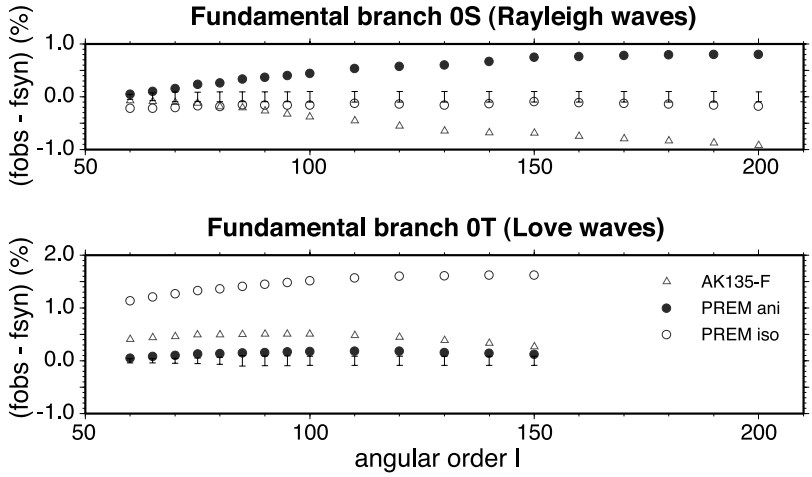

Figure 8. Difference between observed (REM Web page, http://mahi.ucsd.edu/Gabi/rem.html) and predicted fundamental branch mode frequencies for (top) spheroidal and (bottom) toroidal modes with angular orders higher than 60. The data with error bars are compared with predicted frequencies of anisotropic PREM (solid circles), isotropic PREM (open circles), and AK135-F (triangles).

cannot compute the misfit for AK135, as that model does not include a density or anelasticity model, required for computing normal mode frequencies. It is interesting to note that none of the three models fits the observed modal frequencies within the error boundaries of the observations, where it needs to be added that we use an expanded data set compared to what was used in constructing these models.

[32] There is no anisotropy in our physical reference models, so we do not expect to find as good a misfit as anisotropic PREM. We decided as a compromise that the selected (isotropic) pyrolite models are required to have a combined mode misfit (Rayleigh+Love) less than isotropic PREM and a spheroidal misfit less than anisotropic PREM. Figure 9 shows the misfit characteristics for the 12,036 models that pass the first step; 1932 models out of the 12,036, i.e., slightly less than 2% of the original 100,000, pass the step 2 selection criteria for the normal mode misfit.

3.4. Step 3: Combined Body Wave and Mode Data Fit

[33] In Figure 10 the overall (*P* and *S*) travel time fit to transition zone structure and the fit to mode frequencies (spheroidal and toroidal) are compared. There is no correlation between the two fits. Many pyrolite models with a good fit for mode data have a bad fit for travel time data at far-regional distances and vice versa. A few models have a slightly better overall travel time fit than AK135 at these distances, because they fit *S* travel times a bit better. As expected, also only a few models do better than isotropic PREM in fitting the modes. However, we are able to find some models that have a satisfactory fit to all types of data. We define the fit as satisfactory, if the models pass both the mode and the travel time criteria discussed earlier (i.e., less travel time residual shape than PREM and mode fits as well as or better than anisotropic PREM for spheroidal modes and a combined misfit less than isotropic PREM). We obtain 99 best fit models.

[34] Note that this is only 0.1% of the original 100,000 models we generated. We believe that this result is representative of the solution to our inverse problem, as the result is stable for subsets of our model space. It appears to indicate that although possible, it is difficult to reconcile a pyrolitic mantle with global seismic data, given the current mineral physics constraints. However, because a more exhaustive search of the model space is not possible at the moment, we cannot statistically assess the significance of the small number of models accepted. It should be noted that by randomly searching the parameter space we may also include parameter combinations that might be rejected a priori on thermodynamic considerations. This would somewhat shrink our model space, and thereby increase the percentage of accepted models. Other uncertainties, e.g., due to the phase diagrams, associated with the pressure and temperature extrapolation of the mineral data, as well as significant uncertainties in attenuation should be further evaluated. With improving data, it may also become possible to assign non-Poissonian probability distributions to the mineral physics parameters within their uncertainty bounds, and even to preferred combinations of certain parameters, which would affect the solution selection and its significance assessment.

3.5. Solution Characteristics: Mineral Parameters

[35] For all the elastic parameters varied in the inversion, the selected solutions at the different steps in the procedure are shown in Figure 11. The distribution of the thermal expansion coefficients is represented by its first coefficient only (α_0). Variations in thermal expansivity were included as $\alpha \pm 20\%$ in overall values [*Cammarano et al.*, 2003]. The K'' and G'' parameters for lower mantle minerals (below 660) are not reported. No systematic variation in the selection of these parameters was found for the depth range analyzed here. The few parameters for which the inversion showed systematic preferences are highlighted. The mode data prefer a very similar parameter distribution as the step 1

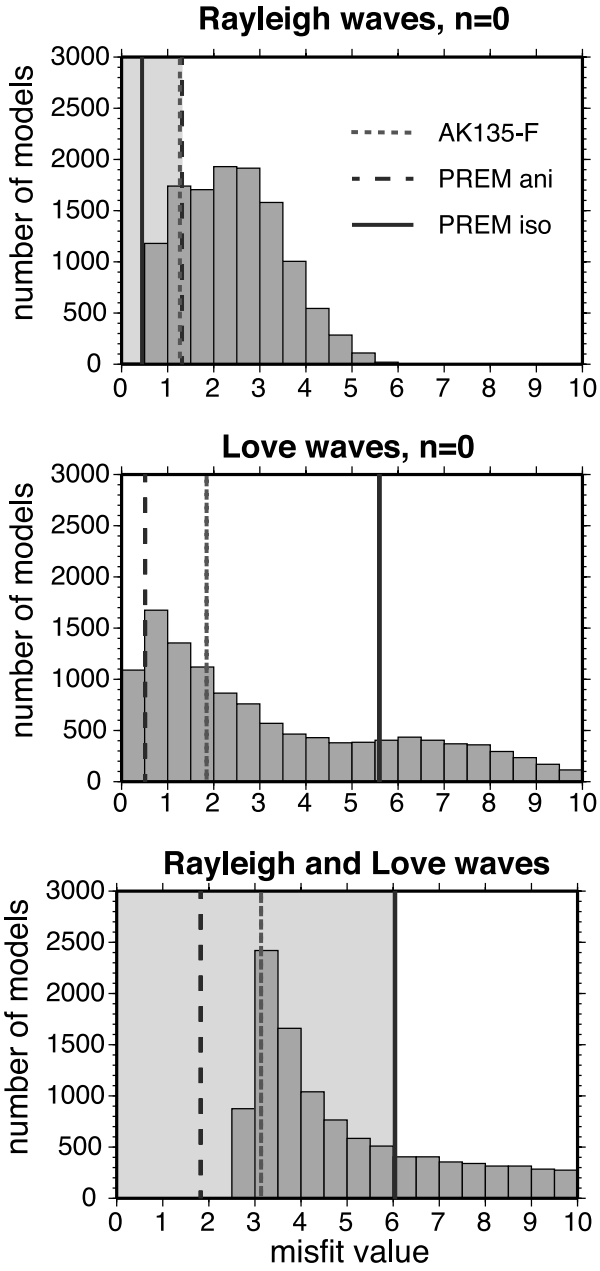

Figure 9. Misfit of all 100,000 models for (top) only spheroidal modes (n = 0, l > 60), (middle) only toroidal modes (n = 0, l > 60), and (bottom) combined, compared with anisotropic PREM (long-dashed line), isotropic PREM (solid line) and AK135-F (short-dashed line). Gray areas mark the criteria applied for accepting models.

family of 12,036 models, i.e., no other values are preferred than those obtained from the constraints on velocity average and "410" and "660" jumps. The travel time data show stronger selectivity, sometimes strengthening the trends defined by the step 1 and mode selections (e.g., for wadsleyite shear modulus parameters), but in some cases also opposing the trends, see for example dK/dT of wadsleyite and ringwoodite or K′ of ringwoodite. The olivine shear modulus and its derivatives, as well as olivine expansivity are on the high side of the uncertainty range. Relatively low values for the same parameters for wadsleyite are preferred by the seismic data. This reduces the jump across the olivine-wadsleyite transition and is preferred in all steps of the procedure. If larger bounds than the ones constrained by Shearer's compilation are allowed, these trends are similar, with the exception of the preference for high olivine shear properties, which is less strong than in shown in Figure 11. The average velocity constraints require relatively low velocities for both wadsleyite and ringwoodite to offset the large jump at 410, resulting in some systematic preferences also for the ringwoodite parameters (Figure 11). In addition, the travel times prefer transition zone gradients that are on the strong side of the step 1 model family. Perovskite and magnesiowüstite parameters reflect that models with jumps at 660 on the high end of the mineral physics data space are preferred.

[36] Although the mode data have no apparent strong preferences for certain elastic parameter values, they do have a strong preference for anelasticity models Q1 and Q5 (Figure 12). Both these models have a temperature and pressure dependence that is cast in terms of the homologous temperature (T/T_{melt}) [*Cammarano et al.*, 2003], which introduces a relatively strong high-attenuation zone at depths less than 200 km, and mild gradients, with cusps at the phase transitions, below. It may seem puzzling that models Q1 and Q5, rather than the almost coincident Q2 and Q5 (or Q1 and Q4), are preferred. Although they give very similar Q values along a 1300°C adiabat, Q2 and Q5 may actually result in more significant differences in velocity gradients with depth. This may lead to a preference for an overall somewhat lower or higher Q value when the depth dependence is changed. The body wave data have little sensitivity to the anelasticity model used, besides requiring an anelastic contribution to the velocities. The mode data are sensitive to Q due to the large range in frequencies they span. However, apparently the travel time

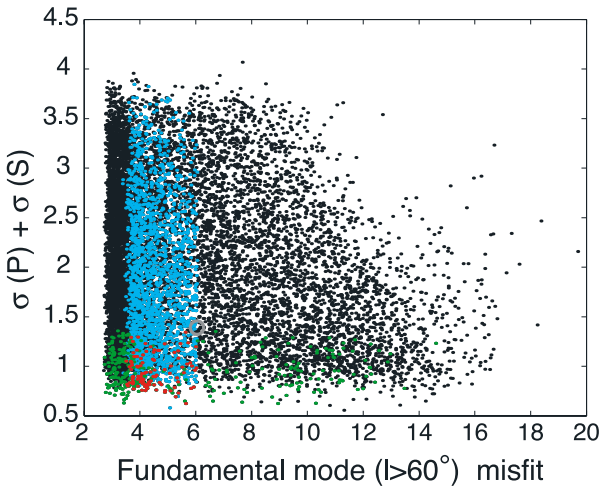

Figure 10. Combined travel time and mode misfit for first selected models (12,036 out of 100,000) in black, best fit models (1932) for mode data in cyan, best fit for travel times (382) in green, and for both data sets (99 models) in red.

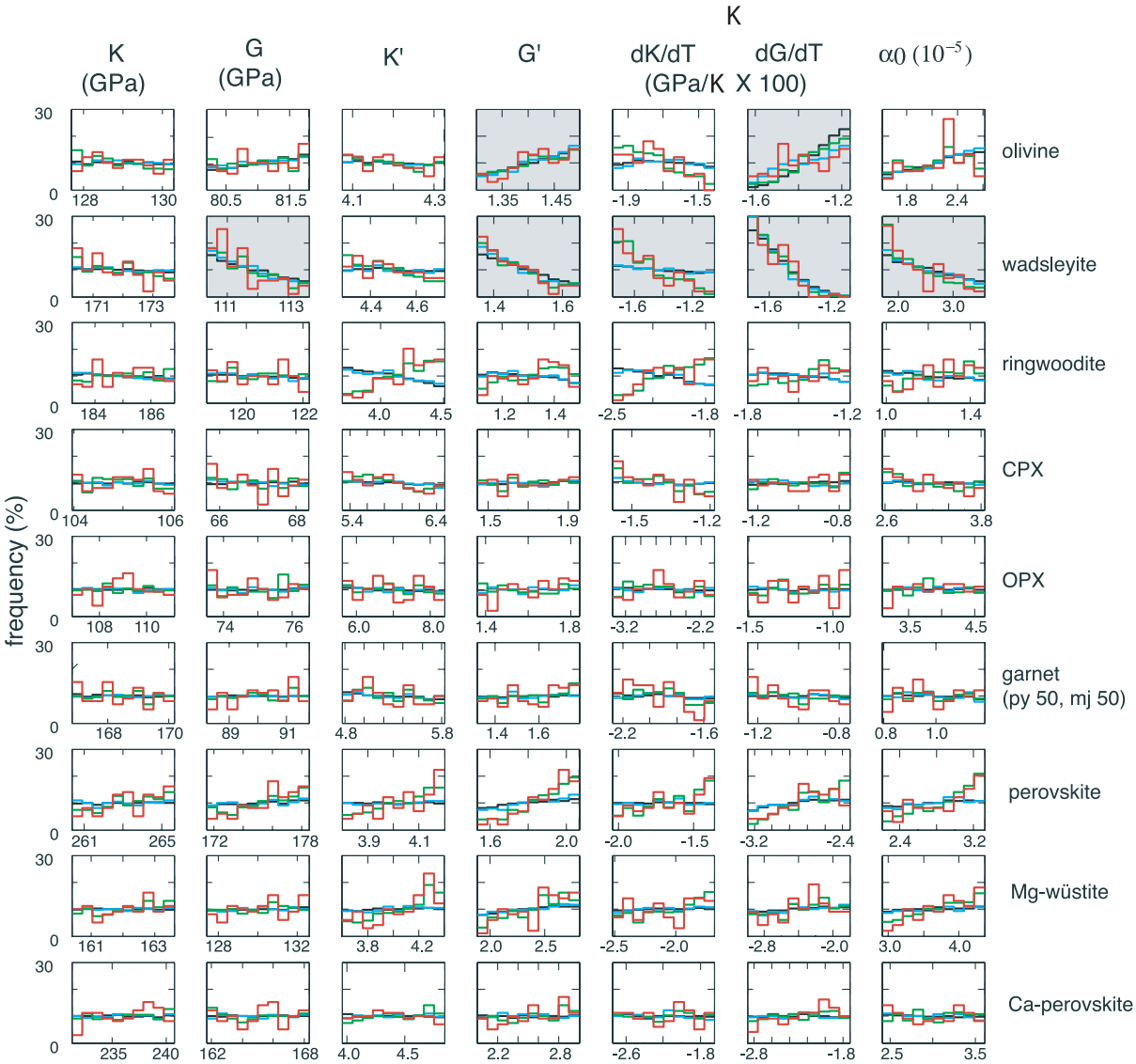

Figure 11. Solution space of the elastic mineral parameters. Shown is the relative frequency of a parameter value within the subset of models left after each selection step: black line, first step (12,036 models); cyan line, second step, best fit to fundamental modes (1932 models); green line, second step, best fit to travel times (382 models); red line, final step, best fit to both data types (99 models). Only the mineral parameters varied are shown (see text).

data do prefer the gradients obtained with model Q5 over those for Q1, resulting in almost half of the final set of models having anelasticity model Q5. Not much significance should be attached to the exact parameter values of the preferred Q models; of main interest are their effects on velocity variation, spatially and with frequency.

[37] We also tested for correlations between different parameters. No clear correlations emerge from the sets of selected models, apart from some correlation between olivine-wadsleyite, wadsleyite-ringwoodite and ringwoodite-perovskite, magnesiowüstite parameters as already indicated in the discussion above, and an anti-correlation between bulk and shear parameters for the same minerals. The limited number of accepted models makes a full exploration of correlations between the 69 elastic parameters difficult. If more models were tested, some other parameter combinations may turn out to be possible too. The strong reduction of the number of accepted models by travel time and mode fits, without significantly narrowing the parameter ranges, implies that only very specific combinations of values of the mineral physics parameters work. The very different possible solutions reflect significant trade-off between different mineral parameters to obtain the same velocity values. This very nonlinear nature of the inverse problem justifies the fully explorative search algorithm chosen.

[38] This paper should be viewed as a first illustration of how a physical reference model can be defined by combining seismic and mineral physics data. There is certainly room for improvement in the inversion procedure and solution evaluation [e.g, *Sambridge*, 1999], as well as in the seismic data set, and mineral physics data and approach. In spite of these limitations, the main results (small number

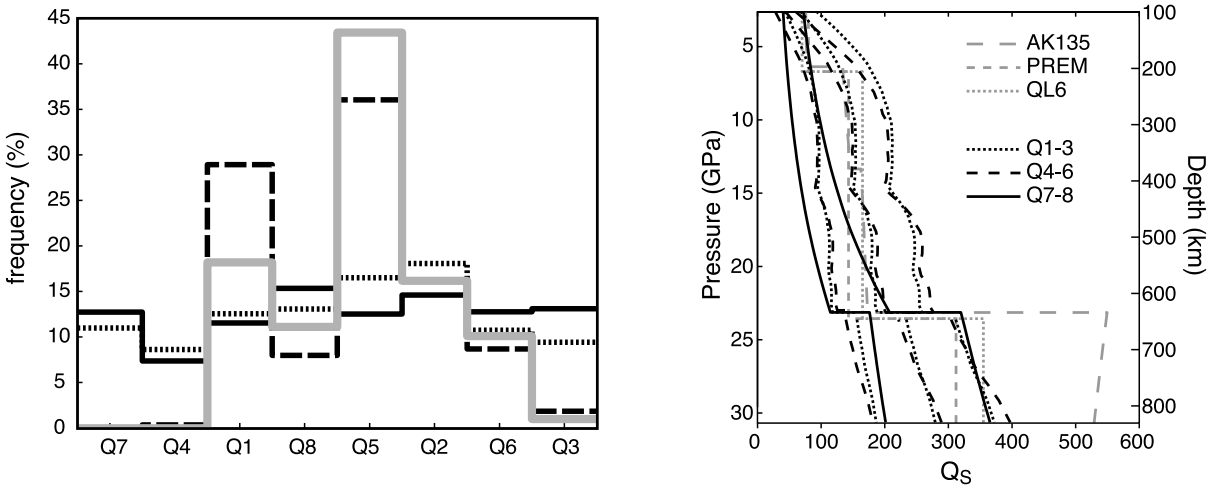

Figure 12. (left) Anelasticity models of the solutions at each step of the inversion (solid line, step 1; long-dashed line, step 2 for modes; short-dashed line, step 2 for travel times; gray line, step 3). (right) Eight anelasticity models used [*Cammarano et al.*, 2003]. These models were constrained by laboratory and seismological data for the upper and shallow lower mantle and are compared with the seismological 1-D attenuation models AK135 [*Montagner and Kennett*, 1996], PREM [*Dziewonski and Anderson*, 1981], and QL6 [*Durek and Ekstrom*, 1996]. Models Q1 through Q3 have the same temperature and pressure dependence but differ in scaling parameter. Models Q4 though Q6 again have the same temperature and pressure dependence, which is stronger than that of Q1–Q3. Q7 and Q8 are two models based completely on experimental data [*Jackson et al.*, 2002]. Travel times have little sensitivity to anelasticity, but the mode data have a strong preference for models Q1 and Q5.

of acceptable parameter combinations, with widely distributed values, with some preference for certain olivine, wadsleyite and ringwoodite parameter values) emerged as robust under all tests we conducted.

3.6. Solution Characteristics: Seismic Profiles

[39] The 99 accepted velocity models look very similar in terms of their absolute velocities (Figure 13). The differences between seismic one-dimensional models are much larger than the differences between the accepted pyrolitic models. Yet, the seismic data are more discriminative than the model comparison seems to indicate. Other, also similarly looking, models were rejected, for example because average upper mantle velocities were not matched close enough. The mineralogical models have a low-velocity and slightly low-density zone at the transition from lithosphere to adiabatic temperature profile around 100 km depth. V_P and V_S are slower than in seismic models (comparable with oceanic PEM [*Dziewonski et al.*, 1975]) above the 410-km discontinuity. Compared to the seismic models, the pyrolite models give a higher velocity below this depth, but a lower average transition zone gradient than PREM or AK135. Above and below the transition zone, all models are subparallel. In the transition zone, some of the *P* models have a slightly negative gradient around the wadsleyite-ringwoodite transition. In V_S one can distinguish models with first a slight decrease and then an increase in velocity gradient, as well as models with a steeper gradient around this transformation. Some of the velocity models even have a slightly low velocity zone around 500 km depth. The pyrolitic models mostly have a somewhat smaller jump at 660 km, especially for V_P, than the seismic models, but a significantly stronger gradient directly below. Note that we do not model the phase transitions in detail and velocities changes linearly within the phase transition interval. Thus no conclusions on sharpness of the transitions should be drawn from Figure 13. This does not affect our analysis, since the seismic data used have no sensitivity to transition width or structure. The small uncertainty bounds on the mineral physics parameters for density results in a tight range of pyrolitic density models. If the mantle is indeed pyrolitic in composition, our analysis gives much tighter constraints on density than seismic data alone can.

[40] The travel time residuals for the final models (Figure 14) have a different shape than those relative to AK135 or PREM but show no larger variations than these models and these variations fall well within the data scatter. The residuals relative to the mode frequency data are shown in Figure 15. Interestingly, most of the models give residuals to the spheroidal modes that fall between anisotropic PREM and AK135-F. The residuals show an increasing underprediction of the mode frequencies with increasing angular order, similar to the misfit trend relative to AK135-F. A few spheroidal fits are comparable to that of isotropic PREM. The toroidal misfits are generally somewhat larger than the misfits of AK135-F and anisotropic PREM, but mostly smaller than those of isotropic PREM. Including anisotropy may improve the fit of the toroidals, as it does in PREM, where however it worsens the spheroidal mode fit.

[41] Overall, in terms of their detailed fit to a similar set of data as was used in constructing PREM and AK135, these 99 models represent acceptable alternative

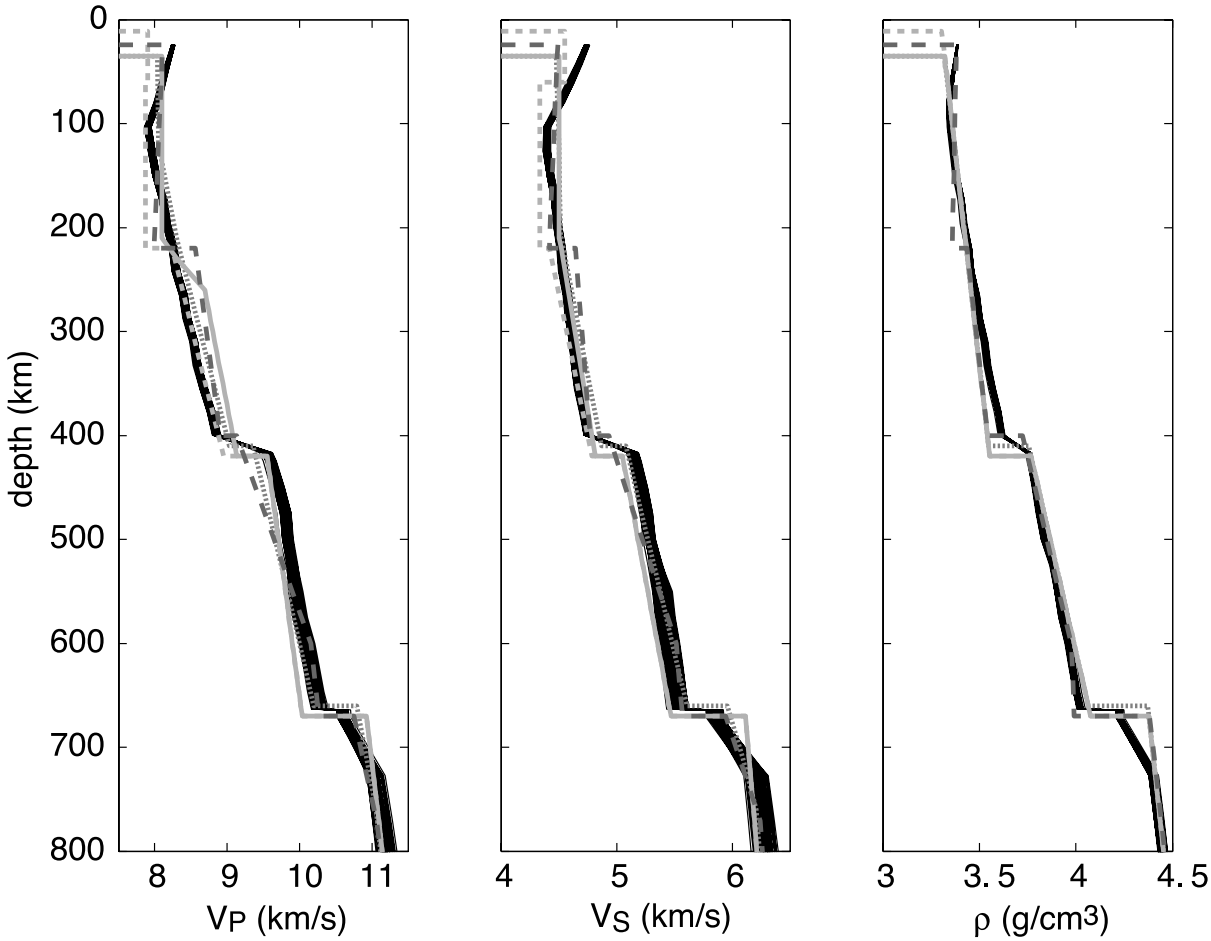

Figure 13. V_P, V_S, and density profiles for the final 99 pyrolite models compared with velocities of AK135 (short-dashed gray line), isotropic PREM (long-dashed dark gray line), and oceanic and continental models PEM-O (medium-dashed gray line) and PEM-C (solid gray line) [*Dziewonski et al.*, 1975].

seismic reference models. Whether the models can also pass more rigorous seismic testing with data sensitive to details of transition zone structure will need to be investigated. The mineral parameters of these models as well as profiles of V_P, V_S, density, Q_P and Q_S will be made available from the first author (see www.sg.geophys.ethz.ch/geodynamics/fabio/PREFum) so that their usefulness can be assessed in seismic inversions and physical interpretation of their results.

4. Conclusions

[42] The data used to constrain the most commonly used seismic one-dimensional Earth models (PREM and AK135) are not very sensitive to detailed structure (jumps and gradients) of the upper mantle and transition zone [*Dziewonski and Anderson*, 1981; *Kennett et al.*, 1995]. This should be kept in mind when attempting physical interpretation of these 1-D models or any 3-D seismic models that were biased or damped toward such reference models. To answer the question whether jumps and gradients in seismic velocity are compatible with a physical interpretation, such as a constant pyrolite composition with phase transitions, and whole mantle convection with an adiabatic temperature profile across 660 km depth, one should therefore perform tests not with seismic models, but with the seismic data.

[43] We presented a first attempt at such an analysis for the upper mantle and transition zone down to 800 km depth. As a physical model we chose a pyrolitic mantle with a temperature profile corresponding to that of 60 m.y. old oceanic lithosphere with below it an adiabat with a potential temperature of 1300°C (i.e., constant composition and whole mantle convection). It has long been recognized that a pyrolitic mantle introduces a stronger jump in velocity at around 410 km depth than included in either AK135 or PREM. Yet we found a set of models within the bounds of available mineral physics data that provides a good fit to far-regional travel times and fundamental spheroidal and toroidal modes. This requires olivine and wadsleyite parameters that minimize the jump near 410 km, and ringwoodite, perovskite and magnesiowüstite parameters that balance upper mantle velocities toward the well-constrained seismic average. Anelasticity models with a mild depth gradient are preferred by the data. Overall, it is possible to fit the seismic data with mineral parameters throughout the entire uncer-

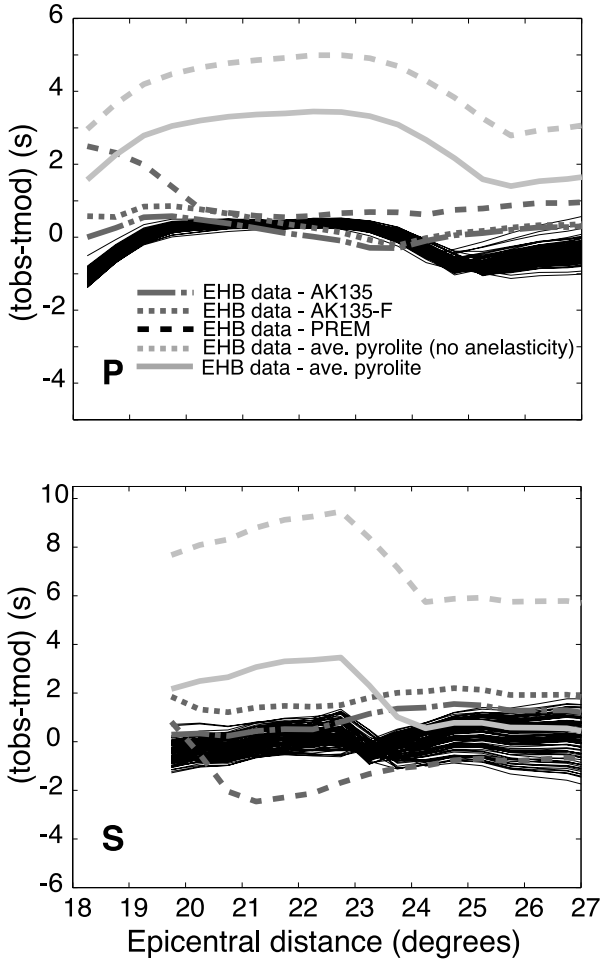

Figure 14. Travel time residuals of the final 99 models.

tainty range, but only a limited number of very specific parameter combinations works. The accepted models are seismically quite similar. They are always slower above and faster below 410 km than AK135 or PREM. Also the transition zone gradient is different from these 1-D seismic models, due to the wadsleyite-ringwoodite transition, and some models even have a slightly low velocity zone at depths around 500 km. To fit both data types, we did need to use a continental-type crust for the ISC travel times (which mainly sample continental structure) while using an average crustal structure (from PREM) for fitting the modes. Future physical reference models might want to include continent-ocean dichotomy at crustal and lithospheric level, like the seismic reference models PEM-O and PEM-C [*Dziewonski et al.*, 1975] did.

[44] Less than 0.1% of the models we tested with a Monte Carlo procedure were accepted. This raises the question whether an adiabatic pyrolitic mantle should not be rejected as a plausible physical 1-D reference structure. Because an exhaustive search was computationally not possible we cannot assess the statistical significance of this small number of acceptable models. However, analyses of model subsets indicate that the results are stable and no much larger percentage of acceptable models would be found if more of the model space was searched. Clear is that acceptable solutions exist and only very specific combinations of mineral physics parameters can reconcile a pyrolitic mantle with the global seismic data. These combinations span almost the full uncertainty range of the mineral parameters however, reflecting the very nonunique relation between velocities and mineral parameters. Tighter constraints on certain parameters (e.g., shear parameters for wadsleyite) would provide indications for or against this physical reference structure. Further work is required to assess the validity of the extrapolation of mineral parameters with pressure and temperature. Seismic data with a much stronger sensitivity to depth variations of transition zone structure (phases reflected or converted at the velocity jumps as well as overtones) and more global body wave sampling (including *PP* and *SS* phases) would also provide more discriminatory constraints.

[45] Although AK135 provides a better fit to *P* wave travel times and PREM provides a better fit to normal mode data, our models fit both data well enough for the models to be useful as seismic reference models. Seismic inversions that would use our set of physical reference models could

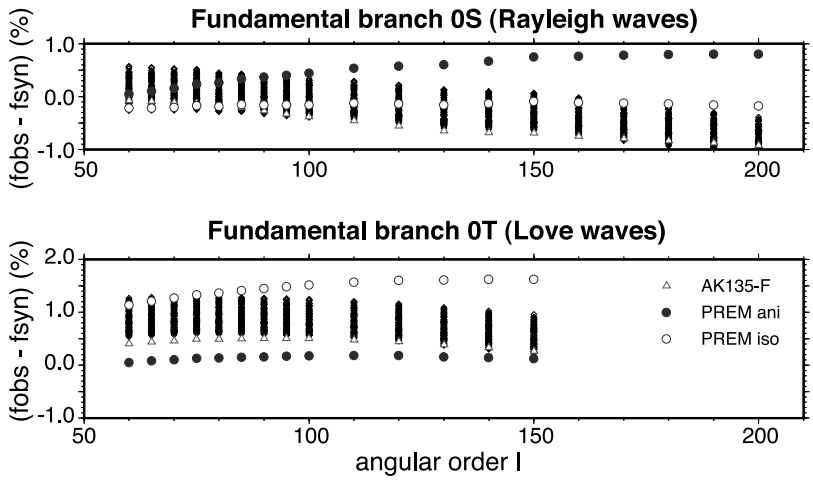

Figure 15. Fundamental mode frequency residuals for the final 99 models for (top) spheroidal and (bottom) toroidal modes.

test whether deviations require extra complexity such as variations in composition and deviations from adiabatic temperatures. Furthermore, the physical reference models have an associated set of mineral parameters that also determine the derivatives of seismic velocities to temperature and composition, facilitating such interpretation. Note that the inversion yields compatible physical models for V_P and V_S, and also provides a reference model for density, even though the seismic data used do not have a very strong sensitivity to density structure.

[46] **Acknowledgments.** We thank E. R. Engdahl for providing the reprocessed ISC catalog, M. Antolik and L. Boschi for providing their summary travel time data set, J. H. Woodhouse for the programs to compute normal mode frequencies and S. van der Lee and J. H. Woodhouse for discussions. Comments from J. Trampert, S. Karato, an anonymous reviewer and J. Ritsema helped us to improve the manuscript. This work was supported by the ETH Zurich, Swiss National Fond (Assistant Professorship SG) and the EUFP5-TMR Network MAGE: MArs Geophysical European Network. This is contribution number 1375 of the Institute of Geophysics, ETH Zurich.

References

Aki, K., and P. G. Richards (2002), *Quantitative Seismology*, 2nd ed., *Univ. Sci. Books*, Herndon, Va.

Antolik, M., G. Ekstrom, and A. M. Dziewonski (2001), Global event location with full and sparse datasets using three-dimensional models of mantle *P* wave velocity, *Pure Appl. Geophys.*, *158*, 291–317.

Bassin, C., G. Laske, and G. Masters (2000), The current limits of resolution for surface-wave tomography in North America, *Eos Trans. AGU*, *81*, Fall Meet. Suppl., Abstract S12A-03.

Bercovici, D., and S. I. Karato (2003), Whole mantle convection and the transition-zone water filter, *Nature*, *425*, 39–44.

Bijwaard, H., and W. Spakman (2000), Non-linear global *P*-wave tomography by iterated linearized inversion, *Geophys. J. Int.*, *141*, 71–82.

Bina, C. R., and G. R. Helffrich (1992), Calculation of elastic properties from thermodynamic equation of state principles, *Annu. Rev. Earth Planet. Sci.*, *20*, 527–549.

Birch, F. (1952), Elasticity and constitution of the Earth's interior, *J. Geophys. Res.*, *57*, 227–287.

Bullen, K. E. (1975), *The Earth's Density*, CRC Press, Boca Raton, Fla.

Cammarano, F., S. Goes, P. Vacher, and D. Giardini (2003), Inferring upper mantle temperatures from seismic velocities, *Phys. Earth Planet. Inter.*, *139*, 197–222.

Cheng, H. X., and B. L. N. Kennett (2002), Frequency dependence of seismic waves attenuation in the upper mantle beneath the Australian region, *Geophys. J. Int.*, *150*, 45–57.

Connolly, J. A. D., and K. Petrini (2002), An automated strategy for calculation of phase diagram sections and retrieval of rock properties as a function of physical conditions, *J. Metamorph. Geol.*, *20*, 697–708.

Deuss, A., and J. H. Woodhouse (2002), A systematic search for mantle discontinuities using SS-precursors, *Geophys. Res. Lett.*, *29*(8), 1249, doi:10.1029/2002GL014768.

Duffy, T. S., and D. L. Anderson (1989), Seismic velocities in mantle minerals and the mineralogy of the upper mantle, *J. Geophys. Res*, *94*, 1895–1912.

Durek, J. J., and G. Ekstrom (1996), A radial model of anelasticity consistent with long-period surface-wave attenuation, *Bull. Seismol. Soc. Am.*, *86*, 144–158.

Dziewonski, A. M., and D. L. Anderson (1981), Preliminary reference Earth model, *Phys. Earth Planet. Inter.*, *25*, 297–356.

Dziewonski, A. M., A. L. Hales, and E. R. Lapwood (1975), Parametrically simple Earth models consistent with geophysical data, *Phys. Earth Planet. Inter.*, *10*, 12–48.

Engdahl, E. R., R. D. van der Hilst, and R. P. Buland (1998), Global teleseismic earthquake relocation with improved travel times and procedures for depth determination, *Bull. Seismol. Soc. Am.*, *88*, 722–743.

Grand, S. P. (2002), Mantle shear-wave tomography and the fate of subducted slabs, *Philos. Trans. R. Soc. London, Ser. A*, *360*, 2475–2491.

Green, D. H., T. J. Falloon, S. M. Eggins, and G. M. Yaxley (1999), Primary magmas and mantle temperatures, *Eur. J. Mineral.*, *13*, 437–451.

Gu, Y. I., A. M. Dziewonski, W. Su, and G. Ekstrom (2001), Models of the mantle velocitiy and discontinuities in the pattern of lateral heterogeneities, *J. Geophys. Res*, *106*, 11,169–11,199.

Gung, Y. C., M. Panning, and B. Romanowicz (2003), Anisotropy and lithospheric thickness, *Nature*, *422*, 707–711.

Helffrich, G. R., E. Asencio, J. Knapp, and T. J. Owens (2003), Transition zone structure in a tectonically inactive area: 410 and 660 km discontinuity properties under the northern North Sea, *Geophys. J. Int.*, *155*, 193–199.

Irifune, T., and A. E. Ringwood (1987), Phase transformations in primitive MORB and pyrolite compositions to 25 GPa and some geophysical implications, in *High-Pressure Research in Mineral Physics*, *Geophys. Monogr. Ser.*, vol. 39, pp. 231–242, AGU, Washington, D. C.

Irifune, T., et al. (1998), The postspinel phase boundary in Mg_2SiO_4 determined by in situ X-ray diffraction, *Science*, *279*, 1698–1700.

Ita, J., and L. Stixrude (1992), Petrology, elasticity and composition of the mantle transition zone, *J. Geophys. Res.*, *97*, 6849–6866.

Jackson, I. (2000), Laboratory measurements of seismic waves dispersion and attenuation: Recent progress, in *Earth's Deep Interior: Mineral Physics and Tomography From the Atomic to the Global Scale*, *Geophys. Monogr. Ser.*, vol. 117, pp. 265–289, AGU, Washington, D. C.

Jackson, I., and S. M. Ridgen (1998), Composition and temperature of the Earth's mantle: Seismological models interpreted through experimental studies of Earth materials, in *The Earth's Mantle: Composition, Structure and Evolution*, edited by I. Jackson, pp. 405–460, Cambridge Univ. Press, New York.

Jackson, I., J. D. Fitz Gerald, U. H. Faul, and B. H. Tan (2002), Grain-size-sensitive seismic wave attenuation in polycrystalline olivine, *J. Geophys. Res*, *107*(B12), 2360, doi:10.1029/2001JB001225.

Karato, S. I. (1993), Importance of anelasticity in the interpretation of seismic tomography, *Geophys. Res. Lett.*, *20*, 1623–1626.

Karato, S. I. (1998), Seismic anisotropy in the deep mantle, boundary layers and the geometry of mantle convection, *Pure Appl. Geophys.*, *151*, 565–587.

Karato, S. I., and B. B. Karki (2001), Origin of lateral variation of seismic wave velocities and density in the deep mantle, *J. Geophys. Res*, *106*, 21,771–21,783.

Katsura, T., et al. (2004), Olivine-wadsleyite transition in the system (Mg, Fe)$_2SiO_4$, *J. Geophys. Res.*, *109*, B02209, doi:10.1029/2003JB002438.

Kennett, B. L. N., E. R. Engdahl, and R. P. Buland (1995), Constraints on seismic velocities in the Earth from travel times, *Geophys. J. Int.*, *122*, 108–124.

Leven, J. H., I. Jackson, and A. E. Ringwood (1981), Upper mantle seismic anisotropy and lithospheric decoupling, *Nature*, *289*, 234–239.

Liebermann, R. C. (2000), Elasticity of mantle minerals (experimental studies), in *Earth's Deep Interior: Mineral Physics and Tomography From the Atomic to the Global Scale*, *Geophys. Monogr. Ser.*, vol. 117, pp. 181–199, AGU, Washington, D. C.

Masters, G., G. Laske, H. Bolton, and A. M. Dziewonski (2000), The relative behavior of shear velocity, bulk sound speed, and compressional velocity in the mantle: Implications for chemical and thermal structures, in *Earth's Deep Interior: Mineral Physics and Tomography From the Atomic to the Global Scale*, *Geophys. Monogr. Ser.*, vol. 117, pp. 63–87, AGU, Washington, D. C.

Mattern, E., J. Matas, J. Bass, Y. Ricard, and J. M. Jackson (2003), Inversion for lower mantle composition and temperature from elasticity parameters and thermodynamic modeling, *Eos Trans. AGU*, *84*, Fall Meting Suppl., Abstract T21F-02.

Montagner, J. P., and B. L. N. Kennett (1996), How to reconcile body-wave and normal-mode reference Earth models?, *Geophys. J. Int.*, *125*, 229–248.

Mooney, W. D., G. Laske, and G. Masters (1998), CRUST 5.1: A global crustal model at $5^\circ \times 5^\circ$, *J. Geophys. Res*, *103*, 727–747.

Oki, S., Y. Fukao, and M. Obayashi (2004), Reference frequency of teleseismic body waves, *J. Geophys. Res.*, *109*, B04304, doi:10.1029/2003JB002821.

Ringwood, A. E. (1975), *Composition and Petrology of the Earth's Mantle*, McGraw-Hill, New York.

Ritsema, J., H. J. van Heijst, and J. H. Woodhouse (2004), Global transition zone tomography, *J. Geophys. Res.*, *109*, B02302, doi:10.1029/2003JB002610.

Röhm, A. H. E., R. K. Snieder, S. Goes, and J. Trampert (2000), Thermal structure of continental upper mantle inferred from *S* wave velocity and surface heat flow, *Earth Planet. Sci. Lett.*, *181*, 395–407.

Saltzer, R. L., R. D. van der Hilst, and H. Karason (2001), Comparing *P* and *S* wave heterogeneity in the mantle, *Geophys. Res. Lett.*, *28*, 1335–1338.

Sambridge, M. (1999), Geophysical inversion with a neighbourhood algorithm—II. Appraising the ensemble, *Geophys. J. Int.*, *138*, 726–746.

Sambridge, M., and K. Mosegaard (2002), Monte Carlo methods in geophysical inverse problems, *Rev. Geophys.*, *40*(3), 1009, doi:10.1029/2000RG000089.

Shearer, P. M. (2000), Upper mantle seismic discontinuities, in *Earth's Deep Interior: Mineral Physics and Tomography From the Atomic to the Global Scale*, *Geophys. Monogr. Ser.*, vol. 117, pp. 115–131, AGU, Washington, D. C.

Shim, S.-H., T. S. Duffy, and G. Shen (2001), The post-spinel phase boundary in Mg_2SiO_4 and its relation to the 660-km seismic discontinuity, *Nature*, *411*, 571–574.

Shito, A., S. Karato, and J. Park (2004), Frequency dependence of Q in Earth's upper mantle inferred from continuous spectra of body waves, *Geophys. Res. Lett.*, *31*, L12603, doi:10.1029/2004GL019582.

Sobolev, S. V., H. Zeyen, U. Granet, C. Achauer, F. Bauer, F. Werling, R. Altherr, and K. Fuchs (1997), Upper mantle temperatures and lithosphere-asthenosphere system beneath the French Massif Central constrained by seismic, gravity, petrological and thermal observations, *Tectonophysics*, *275*, 143–164.

Stixrude, L. (1997), Structure and sharpness of phase-transitions and mantle discontinuities, *J. Geophys. Res*, *102*, 14,835–14,852.

Weidner, D. J. (1985), A mineral physics test of a pyrolite mantle, *Geophys. Res. Lett.*, *12*, 417–420.

Woodhouse, J. H. (1988), The calculation of the eigenfrequencies and eigenfunctions of the free oscillations of the Earth and the Sun, in *Seismological Aogorithms: Computational Methods and Computer Programs*, edited by D. J. Doomboos, pp. 321–370, Elsevier, New York.

Xu, F., J. E. Vidale, and P. S. Earle (2003), Survey of precursors to P'P': Fine structure of mantle discontinuities, *J. Geophys. Res.*, *108*(B1), 2024, doi:10.1029/2001JB000817.

F. Cammarano, Berkeley Seismological Laboratory, 215 McCone Hall, University of California, Berkeley, CA 94720-4760, USA. (fabio@tomo.ig.erdw.ethz.ch)

D. Giardini and S. Goes, Institute of Geophysics, ETH Zürich, Hönggerberg, HPP-O9, CH-8093 Zürich, Switzerland.

A. Deuss, Institute of Theoretical Geophysics, Cambridge University, Downing Street, Cambridge CB2 3EQ, UK.